The 2025 World Congress on
Advances in Structural Engineering and Mechanics (ASEM25)
BEXCO, Busan, Korea, August 11-14, 2025

Monitoring Ground Settlement of Seoul Metro Using SBAS-InSAR

[*]Hahyun Kim[1)], Lang Fu[2)], Taeyong Park[3)], Inyoung Lee[4)], Jeongeun Kim[5)], Hyungjoon Seo[6)]

[1), 3), 4), 5), 6)] *Department of Civil Engineering, Seoul National University of Science and Technology, SEOUL, 01811, Korea*
[2)] *Department of Civil and Environmental Engineering, University of Liverpool, UK L69 7ZX, UK*

[1)] hahyun0214@seoultech.ac.kr [2)] L.Fu8@liverpool.ac.uk
[3)] phnty00@seoultech.ac.kr [4)] ily5984@seoultech.ac.kr
[5)] lkk109s@naver.com [6)] hjseo@seoultech.ac.kr

ABSTRACT

Ground settlement can occur in subway tunnel excavation areas due to various factors, and the possibility of settlement is higher in areas where deep tunnels exist, such as Line 9. However, the existing survey method has limitations in long-term monitoring of a wide area. Accordingly, the SBAS (Small Baseline Subset) InSAR technique, which can analyze changes in a wide range of areas over a long period of time, and the STL (Statistical Time-Series Learning) technique was introduced to separate and analyze seasonal factors and long-term settlement trends. In this study, using the C-band satellite data of SENTINEL-1, a settlement analysis of the Jamsil area where the settlement problem occurred was conducted every 12 days from February 2017 to January 2025. Through SBAS-InSAR analysis, the surface settlement in the area 918-919 of subway line 9 could be confirmed in time series for about 8 years. As a result, the maximum settlement was found to be -15.4 mm. The results of this study show that long-term surface settlement in a wide area located at the top of the tunnel can be measured.

Keywords: Ground Settlement; SBAS-InSAR; Wavelet Transform; Satellite; Tunnel Excavation

1. INTRODUCTION

Ground settlement can occur in areas where subway tunnels are constructed due to various factors such as ground disturbance from tunnel excavation, groundwater leakage and level changes, soil consolidation, and dynamic loads from infrastructure (Yu 2019). In regions with deep tunnels such as subways, the potential for long-term settlement is significantly higher (Zangerl 2008). Indeed, in certain sections of Seoul Metro Line 9, recurring

---

[1), 3), 4), 5)] Undergraduate Student
[2)] Ph. D Student
[6)] Associate Professor

ground settlement has been reported following its opening, as subway usage increased. Moreover, uneven settlement can cause structural failures such as tunnel joint loosening, segment cracking, and leakage, which may eventually trigger sinkholes (Shirlaw 2003). With advancements in satellite remote sensing technology, InSAR (Interferometric Synthetic Aperture Radar) has emerged as a widely used method for monitoring surface deformation. InSAR is a radar imaging technique that utilizes phase differences between two or more complex SAR images to detect surface displacement with high precision across extensive spatial and temporal scales (Ishikawa 2023). Its ability to detect millimeter-level deformation regardless of weather conditions or optical visibility makes it a valuable complement to traditional GNSS-based ground monitoring systems (Osmanoğlu 2016). InSAR plays a vital role in civil engineering applications, particularly in urban areas, for non-contact, long-term monitoring of settlement, uplift, slope failure, and structural deformation (Kauther 2015). Prior studies have employed InSAR to assess ground settlement caused by excessive groundwater extraction, deformation around subway tunnels, slope instability, and thermal expansion due to urban heat island effects (Grafström 1998). Given its economic efficiency, spatial coverage, and high resolution, InSAR is increasingly recognized as a core tool for early warning systems and infrastructure management strategies (Wright 2004). As a high-performance remote sensing technology, InSAR enables precise detection of ground displacement at the millimeter scale by analyzing phase differences between SAR images acquired at different times (Gesangzhuoma 2025)**.**. Unlike GPS, InSAR allows displacement monitoring in areas where direct measurements are difficult (Wei 2010). However, the technology also has limitations. Maintaining phase coherence over time can be challenging, especially in areas with dense vegetation or low backscatter (such as water bodies), leading to reduced signal quality (Nikaein 2021). Furthermore, accurate displacement measurements require high-resolution DEMs, particularly in areas with complex terrain (Ferretti 1999). To overcome these limitations, advanced techniques such as D-InSAR, PS-InSAR, and SBAS have been developed to improve measurement accuracy (Bayer 2007).

This study utilizes long-term InSAR data (2017–2025) from Seoul Metro Line 9 to perform time series analysis that captures settlement trends, seasonal fluctuations, and anomalies. This comprehensive approach addresses limitations of previous studies and contributes to urban ground stability assessments (Zhang 2024). The findings are expected to support data-driven groundwater management, construction control, and urban planning strategies. Among InSAR techniques, the SBAS (Small Baseline Subset) method has demonstrated strong capabilities for long-term, large-scale monitoring of ground deformation and is particularly effective for quantitative settlement analysis around urban tunnels and underground infrastructure (Zhang 2021).

This study focuses on Phase 3 of Line 9 in Songpa-gu, Seoul, particularly the section between Samjeon Station, Seokchon Gobun Station, and Seokchon Station. Notably, significant settlement was observed near Samjeon Station. To analyze this in detail, 16 observation points around the station were selected, and the SBAS-InSAR technique was applied. The analysis showed that settlement was more pronounced at points closer to Samjeon Station and gradually decreased with distance. Using STL (Seasonal-Trend decomposition based on Loess), the influence of seasonal factors was evaluated, revealing that the ground in this region is sensitive to changes in rainfall and groundwater levels. A correlation analysis between groundwater level fluctuations observed near the Tancheon River and ground settlement revealed a similar trend, suggesting that groundwater variation may be a major contributing factor to local settlement (Aksoy 2008). Furthermore, wavelet analysis between ground settlement and groundwater level, including phase arrow interpretation, indicated that groundwater fluctuations may serve as a potential leading factor contributing to settlement (Zhang 2016).

This study quantitatively identifies the characteristics of ground settlement around urban subway infrastructure and demonstrates the practical applicability of SBAS-InSAR for long-term and wide-area monitoring (Zhao 2016). The results can serve as foundational data for predictive modeling and maintenance systems for underground infrastructure and contribute

to proactive management strategies in soft ground or high-risk urban areas.

2. METHODOLOGY

2.1 SBAS-InSAR

The SBAS-InSAR technique is proposed to overcome the limitations of the traditional differential InSAR (D-InSAR) method, which mainly includes the effects of error sources such as temporal decoherence, spatial decoherence, and atmospheric phase delay on the deformation monitoring results(Berardino et al., 2002; Du et al., 2021). Compared with other time-series InSAR methods, the SBAS technique has relatively low requirements on the number of SAR images and image quality and is able to obtain more reliable surface deformation information even when the data volume is limited. The basic principle of this method is to construct multiple differential interferogram ensembles by combining selected interferogram pairs with shorter spatio-temporal baselines, thus increasing the number of interferograms and effectively suppressing the influence of spatial decoherence. On this basis, the least squares method is used to jointly invert the interferogram ensembles to estimate the time-series displacement of surface deformation, and the error introduced by atmospheric delay is weakened or even eliminated by the singular value decomposition (SVD) method(Tao et al., 2020). Finally, by reconstructing each interferogram ensemble, continuous and physically meaningful surface deformation evolution information of the study area can be obtained.

The basic principle of the SBAS technique is to reorganize and pair N+1 SAR images of the same study area on a time series consisting of a series of SAR images (acquired at to t_0 , t_1 , t_2 ,... , t_N) constitutes a time series, $N+1$ SAR images of the same study area are reorganized and paired according to the spatial and temporal baseline conditions required for interferometric processing, so as to construct M interferograms that satisfy the small baseline requirement. If the Jth interferogram is formed by pairing the SAR image acquired by t_e and t_f now, the differential interferometric phase at a point in the study area can be obtained after the elimination of the flat and terrain phases, and its mathematical expression is shown in Equation (1).

$$\Delta\varphi \approx \varphi(t_f, x) - \varphi(t_e, x) = \frac{4\pi}{\lambda}\left[d(t_f, x) - d(t_e, x)\right] \tag{1}$$

where λ is the wavelength of the radar center; $d(t_f, x)$ and $d(t_e, x)$ are the cumulative deformations in the direction of the radar slant with respect to the reference time t_0; $\varphi(t_f, x)$ and $\varphi(t_e, x)$ correspond to the surface deformation phases caused by $d(t_f, x)$ and $d(t_e, x)$.

The linear model is then used to estimate the deformation of N SAR images, and the equation is as follows:

$$A\Phi = \Delta\Phi \tag{2}$$

where Φ represents the meaning of the deformation phase matrix composed of the SAR image points to be solved at N moments; $\Delta\Phi$ represents the meaning of the matrix composed of the phase values of M differential interferograms; A represents the meaning of the matrix coefficients, $M * N$; Each row of the matrix corresponds to a piece of the interferogram, a column of the matrix corresponds to the SAR image at that moment, the position of the main image is the number of columns +1,and the position of the complex image is the number of columns -1,and the rest are 0. Let $M > N$, and the rank of A is N, then the formula can be obtained by the least squares method as follows(Casu et al., 2006):

$$\Phi = (A^T A)^{-1} A^T \Delta\Phi \tag{3}$$

In the actual monitoring process, the coefficient matrix A is not always a full-rank matrix, the system of equations will have an infinite number of solutions, and the matrix A^TA is a singular matrix, so the problem can be solved using the singular value decomposition method, which is used to solve the system of equations by the SVD method to find out the least-squares solution of the system of equations in the sense of the smallest paradigm. And singular value decomposition of the coefficient matrix A to obtain the corresponding deformation. The workflow of this study is shown in Figure 1.

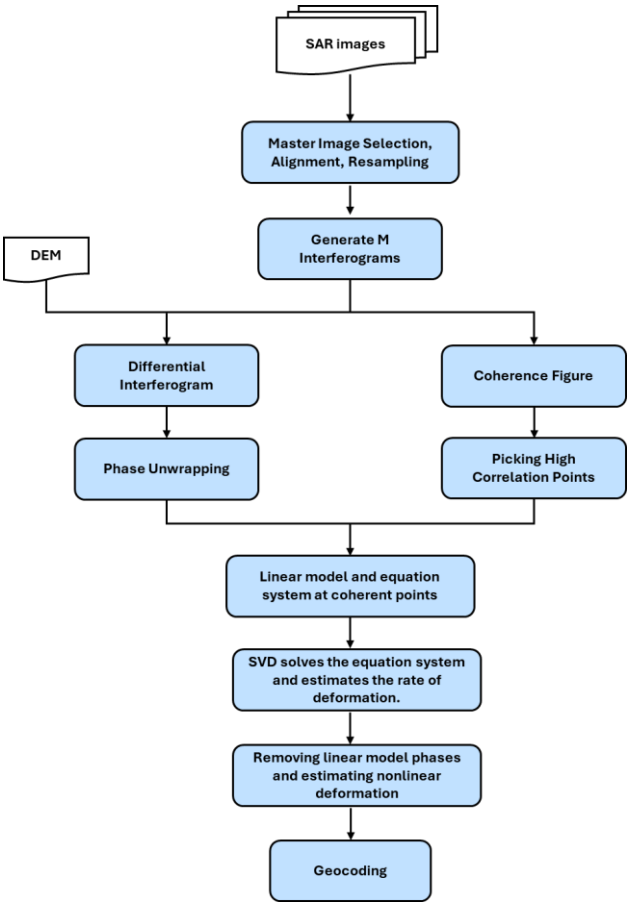

Figure 1. SBAS Workflow

First, by setting reasonable thresholds for the spatial and temporal baselines, image pairs satisfying the conditions are filtered from the multi-temporal phase SAR images to construct an ensemble of small-baseline interferograms with better spatio-temporal coherence. Subsequently, differential interferometric processing is performed on this ensemble to remove the flat phase and terrain phase components, generate the interferogram and perform phase filtering and phase de-wrapping operations to extract the phase information of the target region. Based on obtaining the coherence coefficient map of the interferogram, the regions of high coherence points are extracted, and the linear observation model of the interferometric phase is constructed in these regions. This linear system is solved by the least squares method

combined with singular value decomposition (SVD), which allows the effects of the atmospheric delay difference and the terrain residual phase to be separated and estimated. After removing these interference terms, the surface deformation time series of the target area at each time node is further obtained to realize the continuous monitoring of the slow surface deformation process. Through the joint processing of multi-temporal SAR data, the method transforms the problem of single interferometric shape variation extraction in traditional D-InSAR into a stable least-squares solution process, which not only effectively improves the accuracy and reliability of the results but also enhances its applicability in long time series deformation monitoring.

2.2 STL (Seasonal-Trend decomposition using Loess)

STL (Seasonal-Trend decomposition using Loess) is a widely applied method in time series analysis, which decomposes an original time series into Trend, Seasonal, and Residual components (RB, 1990). Compared to traditional decomposition techniques, STL offers greater flexibility, allowing the adjustment of the seasonal component's variability and the smoothness of the trend component according to the characteristics of the data. This makes it suitable for a wide range of periodic time series. Moreover, the method exhibits strong robustness to outliers, maintaining high decomposition accuracy even in the presence of significant noise. In this study, an additive STL model is employed to decompose the deformation time series, with the general form expressed as follows:

$$U_t = S_t + T_t + R_t \quad t \in [1, N] \tag{4}$$

where U_t is the surface deformation time series data at time t; S_t is the seasonal component at time t; T_t is the trend component of t-deformation; R_t is the residual component of deformation at t time; N is the moment when the deformation time series ends.

The algorithm is structured around nested inner and outer loops. The inner loop is responsible for iteratively estimating and updating the seasonal and trend components. First, during the x^{th} iteration, the previous trend estimate is subtracted to obtain a de-trended sequence:

$$K_t^x = U_t - T_t^{x-1} \tag{5}$$

Then, LOESS is applied to each seasonal subseries to obtain the temporary seasonal component:

$$Temp\ S_t^x = LOESS(K_t^x) \tag{6}$$

The temporary seasonal component is then smoothed and low pass filtered to yield the refined seasonal component:

$$S_t^x = Temp\ S_t^x - L_t^x \tag{7}$$

The trend component is updated by applying LOESS smoothing to the de-seasonalized sequence:

$$T_t^x = LOESS(U_t^x - S_t^x) \tag{7}$$

where $Temp\ S_t^x$ is Temporary Seasonal Component; $LOESS()$ is the series smoothed by applying a locally weighted regression.

The outer loop is designed to enhance the algorithm's robustness to outliers. After each outer iteration, residuals are calculated and weights are assigned to each time point based on residual magnitude, where lower weights indicate potential outliers. Through iterative refinement by inner and outer loops, STL can robustly decompose complex seasonal time

series, and is widely applicable in fields such as ground deformation monitoring, meteorological analysis, and economic forecasting.

2.3 Wavelet Analysis

Wavelet based approaches have become increasingly popular in geosciences for analyzing non-stationary time series with multi-scale variability. While traditional methods such as Fourier analysis provide global frequency information, they lack the ability to resolve the temporal evolution of spectral features. In contrast, wavelet transform offers a time-frequency representation, making it particularly suitable for capturing localized and transient patterns in geophysical signals. In this study, wavelet analysis was employed to investigate the spectral coherence and phase relationship between surface deformation and groundwater level variations, enabling the identification of dominant periodicities and potential lagged responses(Araghi et al., 2017; Komasi et al., 2018).
The cross wavelet transform (XWT) identifies regions in the time–frequency domain where two time series exhibit high common power and stable phase relationships, thereby revealing their potential interdependence. For two time series $A_n$and B_n $(n \in 1,2,3 \dots n)$, the XWT is defined as:

$$W^{(ab)} = W^{(a)}W^{(b*)} \tag{8}$$

where $W^{(ab)}$ is the cross-wavelet power.

WTC is used to identify regions in the time–frequency domain where two time series are coherently related, even if their individual amplitudes differ. It serves as a localized correlation measure in both time and frequency, based on the cross wavelet transform. The wavelet coherence between two series is defined as:

$$R_n^2(S) = \frac{\left|S\left(S^{-1}W_n^{AB}(S)\right)\right|^2}{S(S^{-1}|SW_n^a(S)|^2) \times S\left(S^{-1}\left|SW_n^b(S)\right|^2\right)} \tag{9}$$

where $R_n^2(S)$ varies between 0 and 1. Given two time series A and B, $W_n^a(S)$ and $W_n^b(S)$ by wavelet transform where n is the time index and S is the smoothing opera tor. It is helpful to use wavelet coherence as a local correlation coefficient in the time-frequency space. The smoothing operator S can be expressed as:

$$S_{time} = S_{scale}\left(S_{time}\left(W_n(s)\right)\right) \tag{10}$$

where $S_{scale}$is smoothing along the wavelet scale and S_{time} is smoothing along the time axis.

Several aspects must be considered when interpreting wavelet-based results. The thick black contours in the time–frequency plots represent regions significant at the 5% level based on Monte Carlo testing. The cone of influence (COI), shown as a lighter shaded area, indicates regions where edge effects may distort the results and should be interpreted with caution. In the coherence plots, warm colors (e.g., yellow and red) indicate stronger correlations, while cool colors (e.g., blue) represent weaker(Nazari-Sharabian & Karakouzian, 2020).

3. FIELD TEST

3.1 Introduction of site

The Seoul Subway Line 9 plays a crucial role in the metropolitan transportation network, contributing to the alleviation of traffic congestion in the city center and enhancing

connectivity between major areas. **S**eoul Subway Line 9 began with the opening of Phase 1 in 2009. Currently, it operates 38 stations over a total length of approximately 40.6 kilometers, stretching from Gimpo International Airport Station to VHS Medical Center Station (see Figure 2). The Phase 3 section, which opened in December 2018 and connects Sports Complex Station to VHS Medical Center Station, includes construction zones 918 and 919. Among them, sections 918 and 919 traverse the Songpa-gu and Gangdong-gu areas, which are composed of diverse geological conditions such as alluvium and reclaimed land, increasing the likelihood of differential ground settlement over time. These sections mainly consist of alluvial layers composed of mixed sand, gravel, and silt, making them soft ground with high groundwater levels. In such soft soil, tunnel construction may cause settlement due to soil compression or displacement, thus requiring appropriate countermeasures. Moreover, the areas surrounding the Phase 3 section of Line 9 are densely populated with high-rise apartment complexes and small commercial buildings, and are located near major roads such as Olympic-daero, which necessitates analysis of the impact of traffic-induced ground vibrations on settlement. Additionally, the presence of Seokchon Lake in the vicinity requires careful consideration of the effects of groundwater level fluctuations on ground stability.

Figure 2. 8 stations in 3rd stage section of Line 9

The 918-construction section, undertaken by SK Ecoplant Co., Ltd. (formerly SK Engineering & Construction Co., Ltd.), spans approximately 1,280 meters from Jamsil-dong to Samjeon-dong in Songpa-gu and includes one station and three main ventilation shafts. This section is characterized by loose sandy gravel layers, presenting high construction difficulty. In some areas, buildings are located directly above the tunnel alignment, necessitating thorough ground reinforcement to ensure structural stability during excavation. Accordingly, various reinforcement techniques, such as multi-stage steel pipe grouting and jet grouting, were applied.

The 919-construction section, executed by Samsung C&T Corporation, extends about 1,560 meters from Samjeon-dong to Seokchon Station and includes two stations and seven main ventilation shafts. Due to unstable groundwater levels and weak geological conditions, conventional open-cut construction methods were unsuitable for this section. Therefore, the

shield TBM (Tunnel Boring Machine) method was adopted to ensure safe excavation while minimizing environmental impacts. The area surrounding this section is densely populated with high-rise apartment complexes, small commercial facilities, and major road infrastructure such as Olympic-daero. Additionally, the nearby Seokchon Lake may influence ground settlement through fluctuations in the local groundwater level, which must also be taken into account in the geotechnical assessment.

In Songpa-gu, Seoul, sinkholes were frequently reported not only around the construction site of the Lotte World Tower (Second Lotte World) but also in areas near the Phase 3 construction section of Subway Line 9. Experts have suggested that these phenomena are likely the result of either the combined effects of both projects and the influence of one of them alone. Notably, the 2014 sinkhole incident at the Seokchon Underpass occurred directly above the Line 9 construction area. In 2015, the Seoul Metropolitan Government released a settlement location map of roads surrounding Seokchon Lake, visually indicating ground deformation in Jamsil-dong, Songpa-gu (see Figure 3). Three sites marked by red rectangles on the map represent the locations where settlement was observed. The fact that these events coincided with the timeline of the large-scale Second Lotte World development project suggests the possible influence of groundwater level fluctuations and underground excavation in the region.

Figure 3. Location map of road settlement around Seokchon Lake released by Seoul City in 2015

In addition, multiple ground settlement incidents have been reported in the vicinity of Samjeon-dong, Songpa-gu. Accordingly, this study adopts the SBAS (Small Baseline Subset) InSAR technique to analyze large-scale, long-term surface deformation, along with the STL (Seasonal-Trend Decomposition using Loess) method to distinguish between seasonal and long-term settlement trends. These approaches enable a high-resolution analysis of ground deformation in the vicinity of subway infrastructure.

The Phase 3 section of Line 9 is located near the Han River and is composed of weak strata such as sand and gravel, which are vulnerable to collapse. Compared to other areas, this region has a thinner overburden layer due to the presence of underground roadways, increasing the risk of ground failure. Furthermore, previous investigations have confirmed that adequate ground reinforcement was not conducted, mainly due to design constraints requiring

multiple openings within the underpass structure.
This study focuses on the Jamsil-dong and Seokchon-dong areas in Songpa-gu, Seoul. The three zones marked with yellow lines on the map represent areas potentially affected by ground settlement near the Line 9 extension. Zone 931 (near Samjeon Station) is located in Samjeon-dong, an area densely populated with residential complexes and commercial buildings, raising concerns about settlement due to underground excavation and tunneling. Zone 932 (near Seokchon Gobun Station) includes residential neighborhoods and major roadways. Zone 933 (near Seokchon Station) encompasses the vicinity of Seokchon Lake and the Second Lotte World, where settlement incidents have already been reported in the past. This zone is a key comparison area in this study, as it allows for the observation of the effects of large underground structures and groundwater level fluctuations. The study area is highlighted in yellow on the accompanying map, with the central part marked by a red rectangle (see Figure 4).

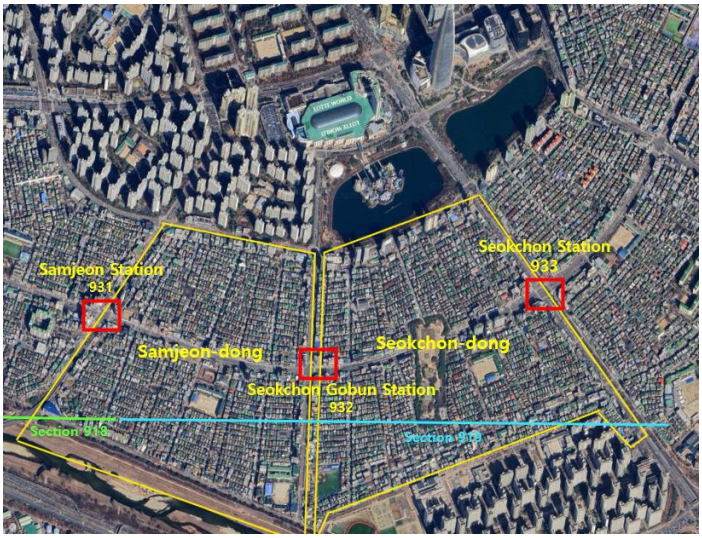

Figure 4. research area

3.2 Data collection

This study utilized C-band Synthetic Aperture Radar (SAR) data acquired from the Sentinel-1 satellite. The imagery was collected in Interferometric Wide (IW) swath mode with VV polarization, and data spanning from February 24, 2017, to January 1, 2025, were used. Sentinel-1 provides regular revisits over the same area, ensuring consistent temporal resolution, which makes it suitable for time-series analysis. All SAR images used in this study were downloaded from the Copernicus Open Access Hub.

To correct the SAR index and define the analysis period, both geometric and temporal baselines between image pairs were considered, and the baseline threshold was limited to less than 300 meters. Interferometric processing was carried out using a combination of ESA's SNAP toolbox and Stanford's StaMPS software. During the phase correction step, a Digital Elevation Model (DEM) was employed to remove topographic phase components and improve interferogram quality through co-registration refinement.

Subsequently, time-series processing was performed using the SBAS algorithm, extracting relative displacement information with respect to a reference image and calculating cumulative subsidence values at each observation point. Coherence analysis of all interferometric pairs

was incorporated into the final interpretation, and a space-time-based deformation map was generated to quantitatively present ground displacement characteristics across the study area.

4. ANALYSIS

4.1 Ground Settlement in Phase 3 area of Line 9

In this study, the SBAS-InSAR (Small Baseline Subset Interferometric Synthetic Aperture Radar) technique was utilized to analyze ground settlement along the construction section of Seoul Subway Line 9, spanning from Samjeon Station to Seokchon Gobun Station and Seokchon Station. Sentinel-1 SAR images collected between 2017 and January 2025 were used in the analysis. The SBAS-InSAR technique was applied to processed imagery to derive the spatial distribution of ground displacement. The results are presented in Figure 5. The analysis revealed that cumulative settlement across the entire study area ranged from –0.21 mm/yr to –0.39 mm/yr, indicating that continuous ground settlement is occurring. As shown in the color-distribution map, areas shaded closer to blue indicate greater magnitudes of settlement. A relatively high rate of settlement was observed in the vicinity of Samjeon Station, suggesting that this area acts as a focal point of settlement within the construction zone. Overall, the analysis clearly distinguishes zones with high settlement risk from more stable areas. These findings can serve as essential baseline data for identifying critical sections that require prioritized management during subway construction and operation to ensure structural safety. Moreover, by providing a quantitative assessment of the spatial distribution and relative magnitude of ground settlement, this study offers useful indicators for future safety inspections and the development of infrastructure maintenance policies.

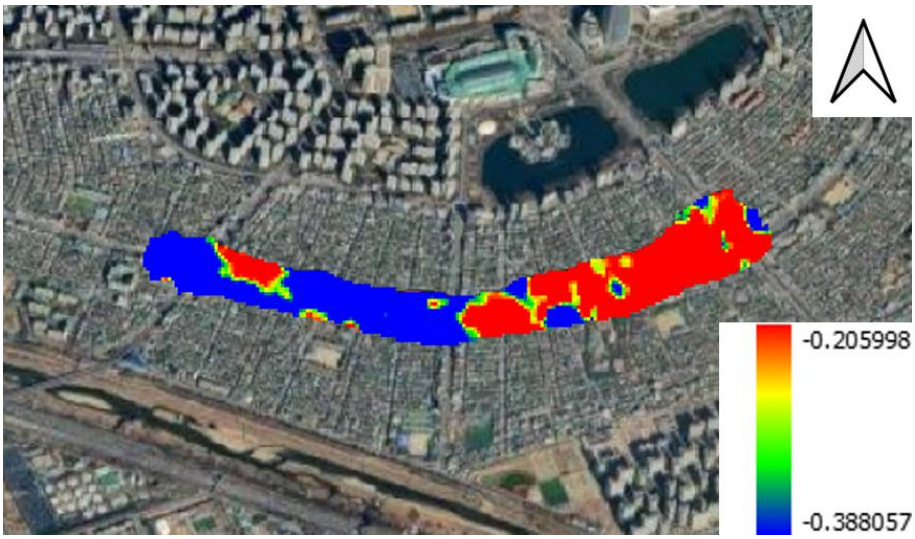

Figure 5. Spatial Distribution of Settlement in Songpa District, Seoul (SBAS-InSAR Analysis Result)

To ensure both spatial continuity of the subway segment and sufficient analytical resolution, a total of 18 observation points were established at 100-meter intervals along the section spanning Samjeon Station, Seokchon Gobun Station, and Seokchon Station for ground deformation analysis (see Figure 6). These evenly spaced points allow for detailed monitoring of subtle variations in ground movement across the entire study area. By maintaining a consistent interval, the dataset ensures a balanced representation of deformation patterns,

minimizing gaps in spatial coverage. This setup facilitates accurate correlation between observed subsidence and potential influencing factors such as construction activities or geological features.

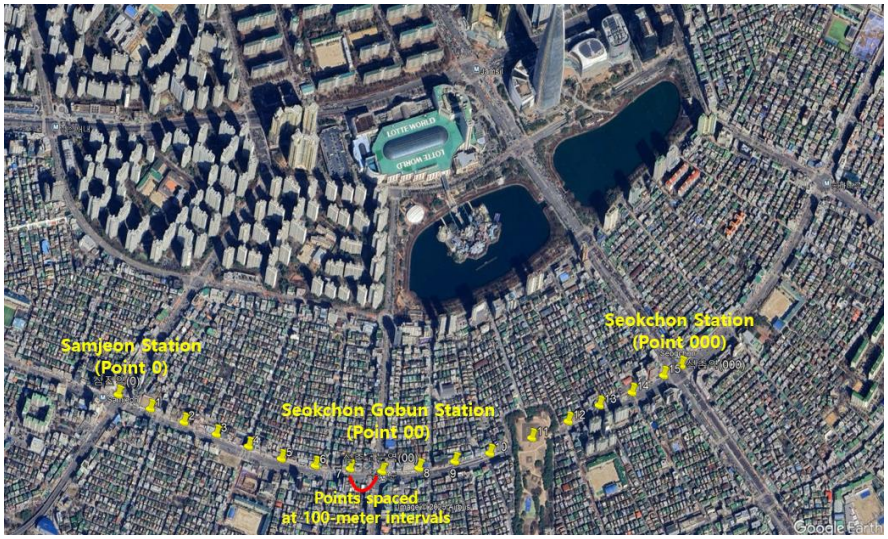

Figure 6. Selection of research points

As a result of the InSAR-based ground displacement analysis performed over the study area, the maximum settlement recorded was -15.4 mm, while the maximum uplift reached 9.61 mm. Throughout the entire analysis section, certain segments consistently exhibited relatively similar settlement trends, indicating localized zones of subsidence (see Figure 7-(a), 7-(b)). Conversely, other segments displayed an overall pattern of ground uplift at comparable levels (see Figure 7-(c), 7(d)). These spatial variations in ground deformation are interpreted to arise from a combination of factors, including the differing geological conditions at each measurement point, fluctuations in the groundwater table, and changes in local surface loads due to construction activities or other anthropogenic influences. Understanding these trends is essential for assessing the stability and safety of the subway infrastructure and for informing future ground management and mitigation strategies. In contrast to these overall spatial settlement patterns, the area surrounding Samjeon Station (Point 0) demonstrated significantly more rapid and pronounced settlement over time compared to other sections (see Figure 7-(e)). Both the settlement rate and cumulative displacement exhibited notable anomalies, indicating statistically significant outliers. Accordingly, a more detailed time-series and spatial analysis was conducted, focusing on the vicinity of Samjeon Station.

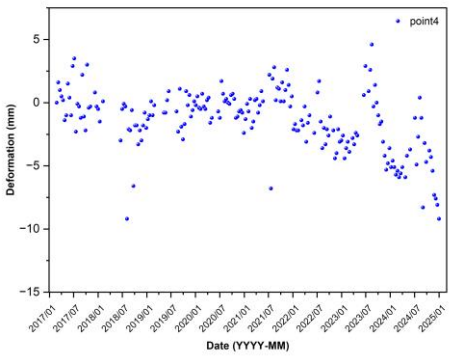

(a) Point 4

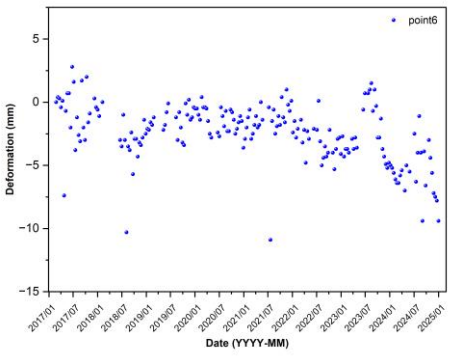

(b) Point 6

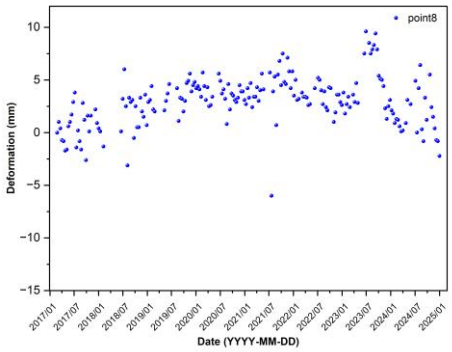

(c) Point 8

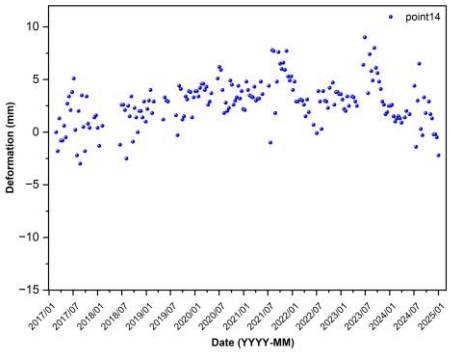

(d) Point 14

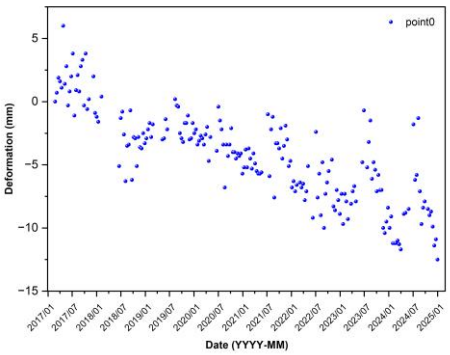

(e) Point 0

Figure 7. settlement trends exhibiting similar patterns across spatial locations

4.2 Settlement around Samjeon Station

Accordingly, this study conducted additional precision analysis to analyze detailed quantitative analysis, cause additional precision analysis, causes additional precision analysis, and temporal change characteristics and temporal change characteristics. In this process, the precision measurement point was performed at approximately 30m intervals, and 16 survey points were selected in this process, and 16 survey points were selected in this process (see Figure 8).

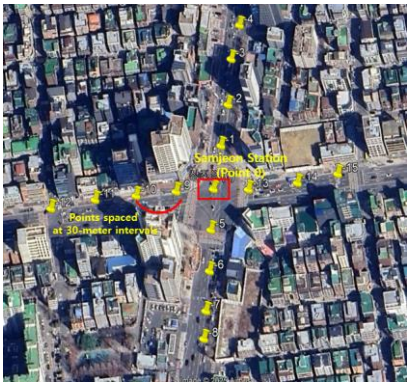

Figure 8. Selection of research points in Samjeon Station

A detailed ground settlement analysis around Samjeon Station (Point 0) revealed a maximum settlement of -15.6 mm and a maximum uplift of 6.8 mm. As shown in Figure 9 and Table 1, a clear spatial trend was identified across the observation points, with more pronounced settlement observed at locations closer to Samjeon Station. These findings suggest that the area around Samjeon Station represents the core zone of settlement within the studied section, and they provide meaningful insights into the spatial extent and boundary of settlement propagation.

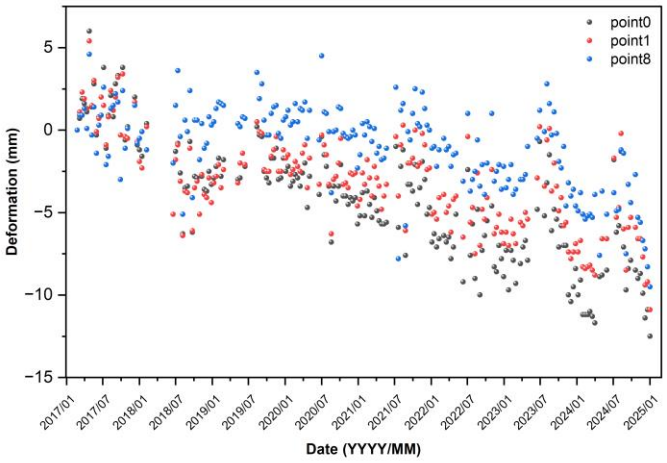

Figure 9. Less settlement tends to decrease as the distance from point0 is greater

Table 1. Settlement decreases with increasing distance from Point 0

(e.g., higher at Points 1, 5; lower at Points 4, 8)

	Point0	**Point1**	**Point5**	**Point4**	**Point8**
Max Deformation (mm)	6	5.4	6.4	4.71	4.6
Min Deformation (mm)	-12.5	-10.9	-13.7	-7.21	-9.5

4.3 Applied time-series decomposition in the area around Samjeon Station

The seasonal-trend decomposition using LOESS (STL) technique decomposes time series data into three components: trend, seasonality, and residences, allowing the characteristics of each element to be analyzed independently. The trend component is used

to identify long-term trends in change, and the flow of data rising or falling over time can be visually confirmed. Through this, the long-term tendency of ground settlement can be clearly identified. The seasonal component explains the pattern of settlement that is repeated periodically due to external environmental factors such as temperature change, precipitation, and groundwater level fluctuations, and is useful for analyzing changes in settlement by year or season. Finally, the residual component represents abnormal changes or outliers that are not explained by trend and seasonality, and may reflect external factors or local influences that are difficult to predict.

The STL technique differs from the existing linear-based decomposition technique in that it gently separates each component using a local regression method based on nonlinear regression. Since this method does not require the assumption of linearity, it may be flexibly applied to unstructured time series data with a complex or irregular structure. In addition, since there is an advantage of being able to set the seasonal cycle flexibly without fixing the seasonal cycle, intuitive interpretation and precise analysis of each component are possible.

In this study, the Seasonal-Trend decomposition using Loess (STL) technique was applied to structurally analyze the complex ground settlement patterns in the three whole areas where settlement was prominent. Through this, it was intended to independently separate and analyze each factor, such as long-term trends, seasonal effects, and abnormal fluctuations (outliers and noise), and to use it as the basis data for improving the accuracy of the future settlement prediction model. For the analysis, data from February 2017 to January 2025 were applied, and the characteristics of each component were evaluated by decomposing the data into three components: trend, seasonality, and residuals through the STL technique.

The first graph, Shape Deform, (see Figure 10-(a)) shows the time series of total settlement during the observation period, and the settlement tends to accumulate continuously from 2017 to 2025. In particular, after 2024, a pattern of marked increase in volatility was observed. Second, (see Figure 10-(b)) the trend component showed a continuous almost linear settlement pattern, suggesting that the section is affected by long-term consolidation. In the seasonal component, (see Figure 10-(c)) periodic settlement fluctuations that are repeated by year appeared, which is interpreted to be due to seasonal changes such as rainfall, groundwater level, and temperature. In particular, it is characterized by the tendency to alleviate intermittent settlement after summer or intensive rainfall. At that point, it was confirmed that the amplitude of the seasonal component was relatively large, which had a significant effect on the overall settlement fluctuation. This suggests that the ground in the entire three regions is sensitive to external environmental factors such as rainfall, temperature, and groundwater level. Finally, (see Figure 10-(d)) the Residuals component represents unexpected outliers and noise components, and most of the values are distributed between -1 and 1, indicating that the explanatory power of the model is high. The predictive performance evaluation of the STL model was performed through the Mean Absolute Error (MAE), Mean Squared Error (MSE), and Root Mean Squared Error (RMSE) indicators, and the smaller the value of all three indicators, the higher the predictive accuracy. As a result of the analysis, the MAE was about 0.08 and the MSE was about 0.4 and the RMSE was about 0.6, which means that the STL model provides a level of prediction accuracy similar to the observed value. In particular, the fact that the RMSE is maintained below 1 strongly suggests that the time series decomposition model effectively explains the settlement data.

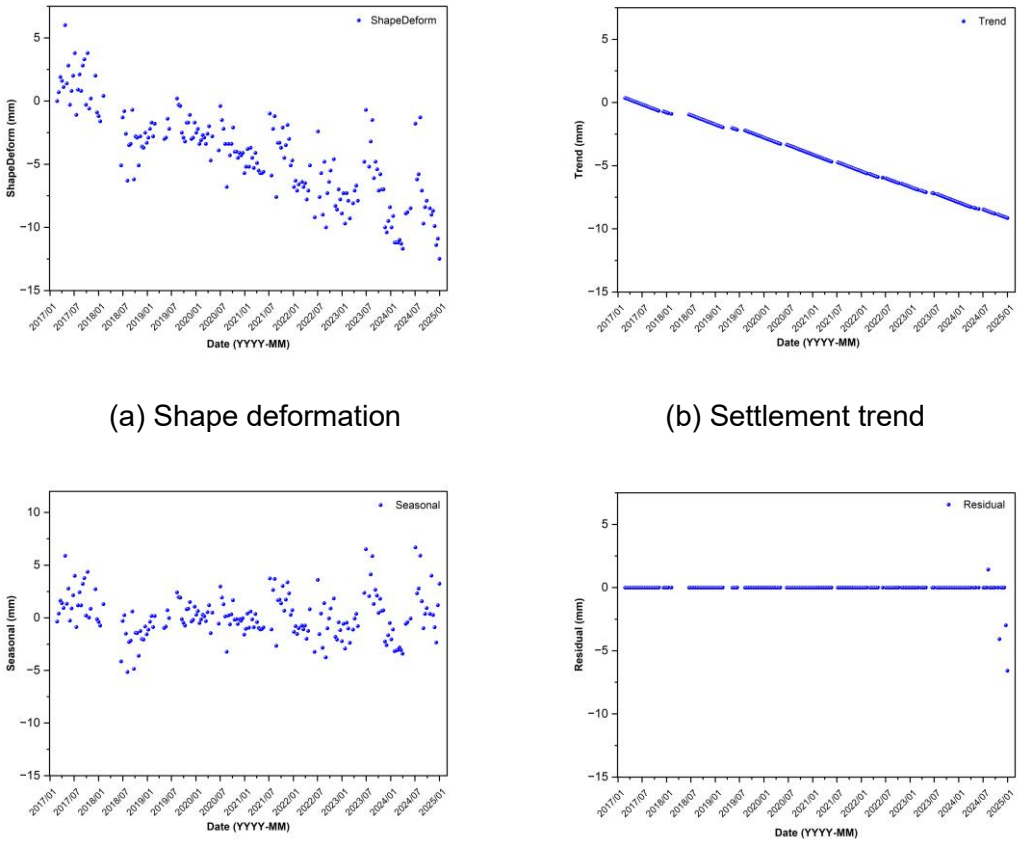

(a) Shape deformation (b) Settlement trend

(c) Seasonal effect (d) Residual effect

Figure 10. STL (Seasonal-Trend decomposition using LOESS) of Samjeon Station

4.4 Groundwater Level and Ground Settlement in the Samjeon Station Area

The time series decomposition results confirmed that the ground near Samjeon Station is highly sensitive to seasonal components. Accordingly, to analyze the correlation between the groundwater level and the ground settlement, the groundwater level data observed in the Tancheon stream site in Songpa-gu, Seoul was additionally used. After a surge in precipitation, the groundwater level tends to rise rapidly in a short period of time, and gradually declines after a delay of a certain period of time after the rainfall is over. This trend suggests a temporary increase in the groundwater level due to rainfall and the resulting buffering effect. Despite repeated rainfall, the groundwater level showed a generally decreasing trend during the observation period, which is interpreted as the effect of continuous groundwater use and the outflow of groundwater. When the groundwater level is lowered, the effective stress in the ground tends to increase, promoting consolidation and accelerating settlement. In particular, in the fine-grained soil layer, the gap narrows due to the outflow of groundwater, and dense settlement clearly occurs. On the other hand, as the groundwater level increases, the gap water pressure increases and the effective stress decreases, and accordingly, the settlement is suppressed. This means that the rise in the groundwater level due to rainfall plays a role of buffering the settlement. As such, it can be seen that the effect of the high and low groundwater level on settlement is a more direct and important measure even under the same precipitation conditions. (Figure 11)

Based on the time series analysis of groundwater levels and settlement conducted from May 1, 2023, to January 31, 2025, the lowest groundwater level during the observation period was recorded on October 22, 2024, at –4.44 m, accompanied by a rainfall of 18.5 mm and a

notably large settlement observed at Samjeon Station (point0). In contrast, on July 15, 2023, the groundwater level reached its highest point at –3.52 m, with only 1 mm of rainfall and relatively minor settlement observed at point0.

These results support that the absolute value and the fluctuation range of the groundwater level have a more important influence on the occurrence of settlement than the precipitation itself. Therefore, monitoring the groundwater level should be considered as a key variable when evaluating ground stability and predicting the settlement.

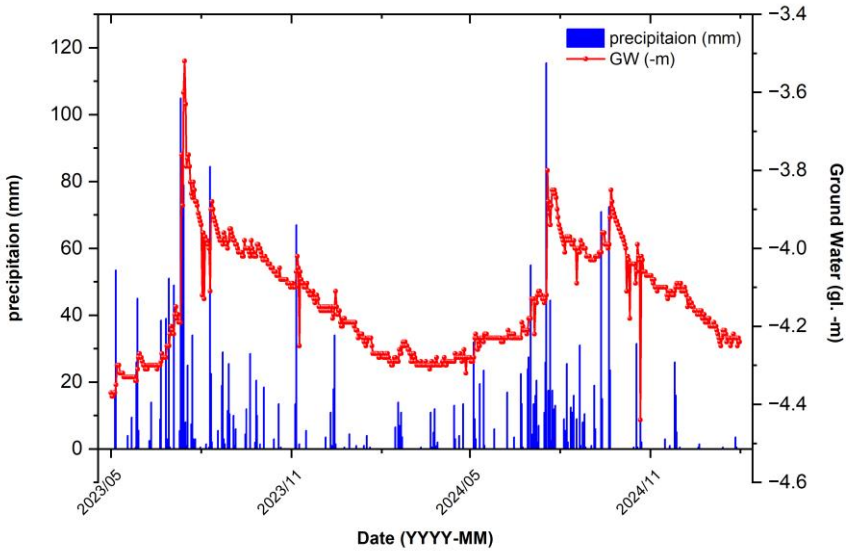

Figure 11. Groundwater level and precipitation

This graph visualizes the ground settlement and ground level fluctuations at a total of 16 points in the Samjeon Station area from May 2023 to January 2025 (see Figure 12). At most points, ground settlement tended to gradually decrease cumulatively over time. Overall, the fluctuation patterns of ground settlement and groundwater level were similar, raising the possibility that the decline of the groundwater level served as a major factor that could cause or facilitate ground settlement. The bold red line in the graph represents the change in groundwater levels. The groundwater level ranges from about -3.7 m to -4.3 m. In particular, between July-August 2023 and July-August 2024, there was a clear tendency for ground settlement to accelerate immediately after a sharp drop in groundwater levels, indicating that seasonal rainfall or changes in water levels may have substantially affected the rate of settlement.

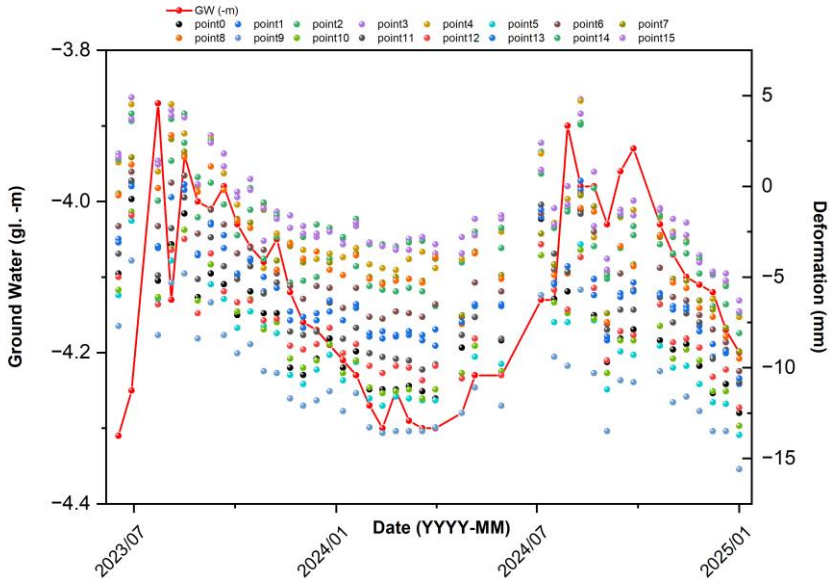

Figure 12. Ground Settlement and Groundwater Level at 16 Monitoring Points

Among the 16 deformation monitoring points analyzed, four representative locations (P5, P7, P14, and P15) exhibited statistically significant coherence with groundwater level fluctuations. As shown in Figure 13-(b), Figure 13-(d), Figure 13-(f) and Figure 13-(h), these points present high wavelet coherence values (generally exceeding 0.7) within the 4–8 period range. Notably, the significant regions, outlined by the 95% confidence contours, are located outside the cone of influence, indicating the robustness of the signal.

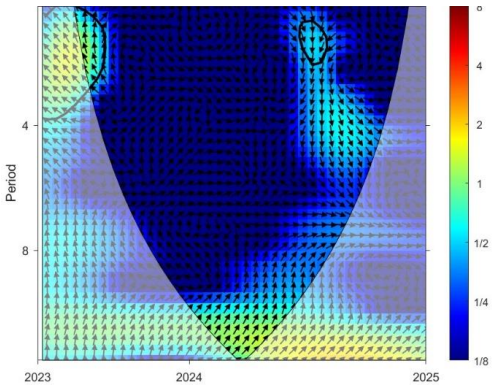

(a) Point 5

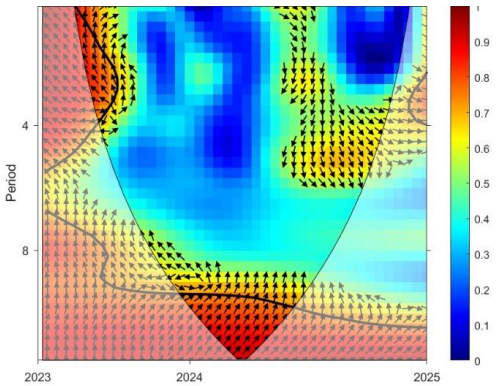

(b) Point 5

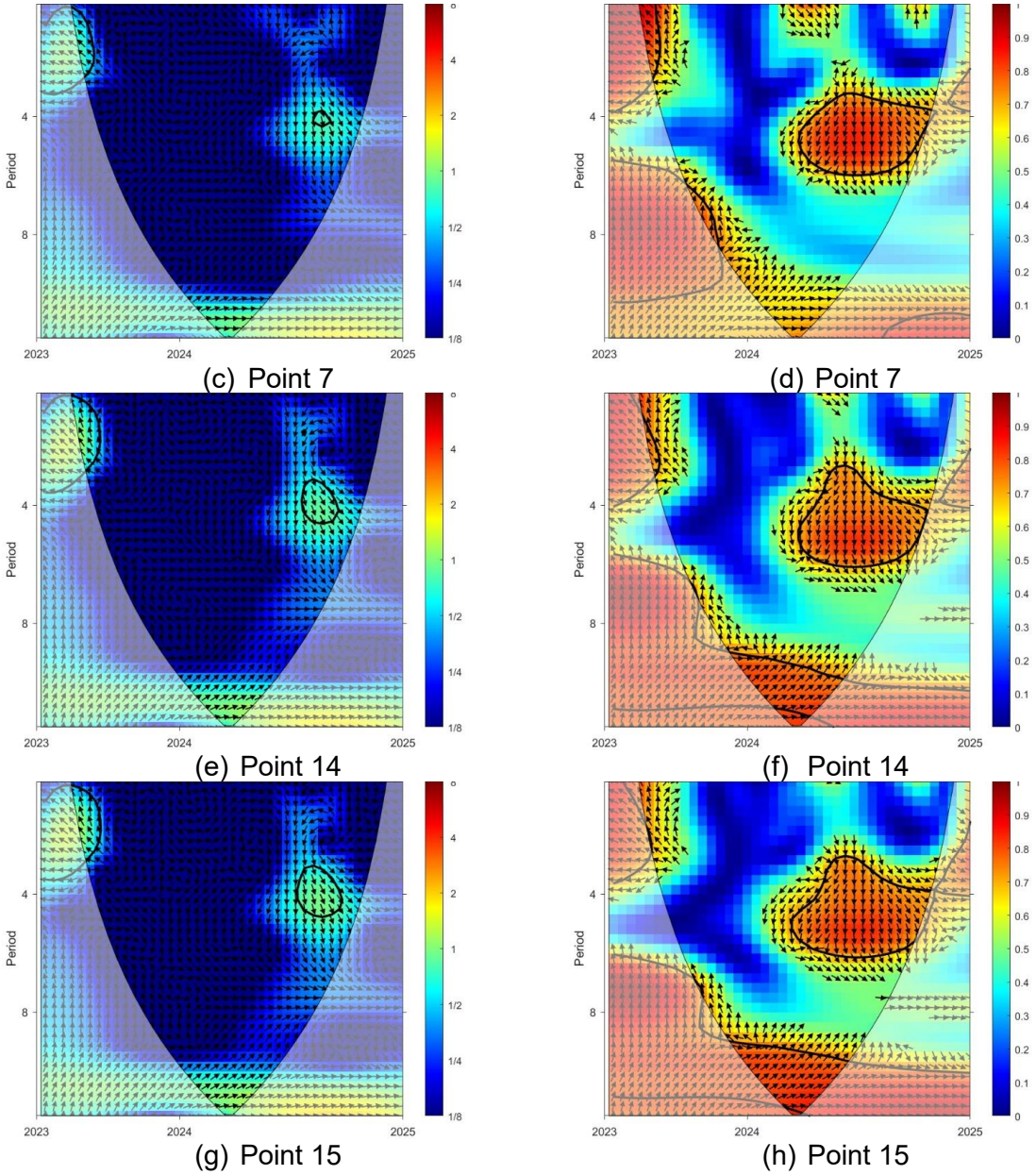

Figure 13. (left) Cross Wavelet Transform, (right) Wavelet Transform Coherence results of P5, P7, P14 and P15

At all four points, the phase arrows within the significant regions are predominantly oriented in the southeast direction, implying a clear phase lag of surface deformation relative to groundwater level changes. This pattern suggests that deformation tends to occur after groundwater drawdown events, potentially due to delayed consolidation or hydraulic response in the subsurface strata. Additionally, the consistency of both XWT energy concentrations and WTC coherence patterns across these points highlights stable coupling behavior within this frequency band (see Figure 13-(a), Figure 13-(c), Figure 13-(e), Figure 13-(g)). These findings demonstrate that, despite the heterogeneity of urban geological conditions, certain locations exhibit pronounced sensitivity to groundwater variations, with deformation responses that are both temporally coherent and physically interpretable.

5. DISCUSSION

This study focuses on the section of Seoul Metro Line 9 spanning from Samjeon Station to Seokchon Gobun Station and Seokchon Station, located in Songpa-gu, Seoul. Line 9, which opened in 2009, comprises 38 stations over approximately 40.6 km. The study area, corresponding to sections 918–919, encompasses a range of geological conditions including alluvial deposits and reclaimed land, which may be susceptible to differential settlement over time. In particular, the area is characterized by mixed alluvial layers of sand, gravel, and silt, and is underlain by soft ground with a high groundwater level. In addition, the proximity of high-rise residential buildings, commercial facilities, and major roads such as Olympic-daero highlights the need for detailed ground deformation analysis.

Accordingly, this study applied the SBAS-InSAR technique to analyze ground settlement in the targeted section. To ensure spatial continuity along the subway corridor and achieve sufficient analytical resolution, a total of 18 observation points were selected at approximately 100-meter intervals, and time-series deformation analysis was conducted. The analysis revealed that certain sections exhibited relatively similar settlement patterns, while other areas showed comparable trends of ground uplift. In contrast, more pronounced settlement was observed near Samjeon Station, indicating that this area may serve as a focal point of ground deformation within the study section.

To conduct a more detailed analysis around Samjeon Station, 16 observation points were selected at approximately 30-meter intervals, and a high-resolution settlement analysis was performed. As a result, the maximum observed settlement reached -15.6 mm, and the degree of settlement was found to increase closer to Samjeon Station, showing a clear inverse relationship with distance. To investigate whether seasonal factors influenced ground settlement in the area, the STL (Seasonal-Trend decomposition using Loess) method was applied. STL decomposes time-series data into trend, seasonal, and residual components, enabling independent analysis of the correlation between each component and ground deformation.

The decomposition results indicated that ground settlement near Samjeon Station is highly sensitive to seasonal variations, suggesting that external factors such as rainfall and temperature changes may influence settlement. The predictive performance of the STL model was evaluated using MAE, MSE, and RMSE indicators, with values of MAE = 0.08, MSE = 0.4, and RMSE = 0.6, indicating that the model provides highly accurate estimates consistent with observed data.

In addition, to assess the correlation between groundwater levels and settlement, groundwater fluctuation data from the Tancheon riverside area in Songpa-gu were visualized alongside settlement measurements near Samjeon Station. Following heavy rainfall, groundwater levels rapidly increased over a short period and then gradually declined after a delay. Despite repeated rainfall events, an overall downward trend in groundwater levels was observed, likely due to continuous groundwater extraction or external outflow.

The comparison between settlement and groundwater variation showed a highly similar temporal pattern, particularly highlighting that settlement tended to accelerate after a sharp decline in groundwater level. To further examine this relationship, WTC (Wavelet Transform Coherence) and XWT (Cross Wavelet Transform) analyses were conducted for the period between late 2023 and early 2025, during which settlement was most significant. The integration of XWT and WTC analyses reveals a clear spectral and temporal coupling between surface deformation and groundwater level changes, particularly in points such as P5, P7, P14, and P15. Coherence values exceeding 0.8 within the 4–8 period band (corresponding to 56–112 days) coincide with high-energy regions in the XWT plots, confirming that deformation responds predominantly to sub-seasonal and seasonal groundwater fluctuations. These time scales align with known recharge-discharge cycles in urban aquifers, reflecting periodic pumping patterns and climate-driven groundwater dynamics.

The southeast-oriented phase arrows consistently observed in both analyses imply a temporal lag of approximately 14–28 days between groundwater decline and subsequent ground settlement. This lag is physically attributed to the time-dependent dissipation of pore pressure and delayed compaction in semi-confined or compressible layers. The shorter lag observed at P7, for instance, may result from shallower aquifers or higher-permeability materials, allowing for a more immediate deformation response. In contrast, the broader and stronger coherence at P14, with a clear two-cycle lag (~28 days), suggests a thicker compressible sequence or slower hydraulic diffusion. Spatial variability among the 16 analyzed further highlights the role of geological and anthropogenic heterogeneity in modulating the deformation response. The absence of significant coherence in most points may reflect either low sensitivity to groundwater change, or overlapping influences from non-hydrological drivers such as loading, tunneling, or thermal expansion. Conversely, the clear coupling observed in the selected points suggests localized susceptibility to hydrologically induced settlement.

Ultimately, the findings underscore that urban ground deformation is, in certain locations, strongly influenced by periodic groundwater changes with measurable lag times. These results offer implications for the monitoring and management of urban aquifers and land settlement and highlight the value of wavelet-based time-frequency analysis in future hydromechanical research. These findings demonstrate that settlement near Samjeon Station is not a simple linear response, but rather a complex phenomenon influenced by various periodic components. This also implies that groundwater dynamics are a potential driving factor behind settlement.

Overall, this study verifies that the SBAS-InSAR (Small Baseline Subset Interferometric Synthetic Aperture Radar) technique is a powerful tool for monitoring long-term ground deformation with high spatial and temporal resolution, particularly suitable for quantitative analysis of subtle settlement around large-scale urban infrastructure. By applying SBAS-InSAR in this study, it was possible to accurately capture the spatial and temporal distribution of settlement based on years of time-series data with wide-area coverage. This method serves as an efficient, non-contact alternative that addresses the limitations of traditional field-based monitoring in terms of time, labor, and cost. Looking ahead, SBAS-InSAR is expected to be widely applicable in fields such as urban underground development, ground stability assessments near subway lines, and settlement prediction model development.

6. CONCLUSION

This study evaluates land settlement in the Songpa District of Seoul, South Korea, using SBAS-InSAR analysis based on InSAR data. The study area encompasses a deep tunnel section of Seoul Subway Line 9, including Samjeon Station, Seokchon Gobun Station, and Seokchon Station. This region is situated on soft ground near the Han River and is characterized by weak geological conditions. In particular, the presence of an underpass has resulted in a thinner upper soil layer compared to surrounding areas, increasing the risk of settlement. Given these ground conditions, a detailed investigation into land settlement was deemed necessary. To this end, observation points were set at regular intervals to assess displacement at each location, and additional analytical techniques were employed for a more in-depth evaluation. The main findings of this study are summarized as follows.

1) In the section encompassing Samjeon Station, Seokchon Gobun Station, and Seokchon Station within the Songpa District, a total of 18 observation points were established at approximately 100-meter intervals for SBAS-InSAR analysis. The results revealed a maximum settlement of –15.4 mm and a maximum uplift of 9.61 mm. In certain segments of the study area, a consistent pattern of settlement was observed, while other segments exhibited a relatively uniform uplift trend. Although general displacement patterns were identified across various sections, the area near

Samjeon Station (Point 0) showed a significantly more pronounced and rapid settlement over time compared to other locations.

2) Accordingly, an additional analysis was conducted to more precisely investigate the pronounced settlement observed near Samjeon Station. A total of 16 observation points were designated at approximately 30-meter intervals centered around Samjeon Station for a more detailed SBAS-InSAR analysis. The results indicated that the closer a point was to Samjeon Station (Point 0), the greater the amount of settlement, whereas settlement gradually decreased with increasing distance from the station.
3) To conduct an in-depth analysis of the Samjeon Station area, a time-series analysis was applied. The results for Samjeon Station (Point 0) revealed periodic variations in settlement across different years. This indicates that land settlement in this area is highly responsive to seasonal factors such as rainfall, groundwater level, and temperature.
4) Based on the results of the time-series analysis, additional groundwater level data observed at the Tancheon riverbed in Songpa District, Seoul, were utilized to analyze the correlation between groundwater levels and land settlement in the vicinity of Samjeon Station. The analysis showed that when the groundwater level reached its lowest point at –4.44 m, the observed settlement was relatively large. In contrast, when the groundwater level was at its highest, at –3.52 m, the settlement was comparatively minor. These findings suggest that groundwater level monitoring should be considered a key factor in evaluating ground stability and predicting settlement.
5) To conduct a more in-depth analysis of the relationship between groundwater levels and land settlement, a wavelet analysis technique was applied. Among the 16 monitoring points near Samjeon Station, four representative points (P5, P7, P14, and P15) exhibited statistically significant consistency between groundwater fluctuations and land settlement. At all four points, the phase arrows pointed in a southeast direction, indicating that settlement tends to occur following a drop in groundwater levels. These findings demonstrate that, despite the heterogeneity of urban subsurface conditions, temporally consistent and interpretable ground deformation in response to groundwater changes can be clearly observed at specific locations.

Acknowledgements

This work was supported by the National Research Foundation of Korea (NRF) grant funded by the Korea government (MSIT) (No. RS-2021-NR060085).

REFERENCE

Yu, L., Zhang, D., Fang, Q., Cao, L., Xu, T., & Li, Q. (2019). “Surface settlement of subway station construction using pile-beam-arch approach”. *Tunnelling and Underground Space Technology,* **90**, 340-356.

Zangerl, C., Evans, K. F., Eberhardt, E., & Loew, S. (2008). “Consolidation settlements above deep tunnels in fractured crystalline rock: Part 1—Investigations above the Gotthard highway tunnel”. *International Journal of Rock Mechanics and Mining Sciences,* **45**(8), 1195-1210.

Shirlaw, J. N., Ong, J. C. W., Rosser, H. B., Tan, C. G., Osborne, N. H., & Heslop, P. E. (2003). “Local settlements and sinkholes due to EPB tunnelling”. *Geotechnical Engineering,* **156**(4), 193-211.

Ishikawa, M., Avtar, R., & Mo, S. (2023). “Using interferometric synthetic aperture rader (InSAR) analysis to detect ground deformation related to irreversibly changing ground ice, Mongolia”. *Land Degradation & Development(LDD),* **34**(9), 2707-2719.

Osmanoğlu, B., Sunar, F., Wdowinski, S., & Cabral-Cano, E. (2016). “Time series analysis of InSAR data: Methods and trends”. *ISPRS Journal of Photogrammetry and Remote*

Sensing, **115**, 90-102.
Kauther, R., & Schulze, R. (2015). “Detection of settlement affecting civil engineering structures by using satellite InSAR”. *Proceedings of the Ninth Symposium on Field Measurements in Geomechanics, Australian Centre for Geomechanics,* 207-218.
Grafström, S., Schuller, P., Kowalski, J., & Neumann, R. (1998). “Thermal expansion of scanning tunneling microscopy tips under laser illumination”. *Journal of Applied Physics,* **83**(7), 3453-3460.
Wright, T. J., Parsons, B. E., & Lu, Z. (2004). “Toward mapping surface deformation in three dimensions using InSAR”. *Geophysical Research Letters*, **31**(1), L01607.
Gesangzhuoma, Han, Z., Cheng, L., Jiang, Z., & Jiang, Q. (2025). “Surface Micro-Relief Evolution in Southeast Tibet Based on InSAR Technology”. *Land,* **14**(3), 503.
Wei, M., Sandwell, D., & Smith-Konter, B. (2010). “Optimal combination of InSAR and GPS for measuring interseismic crustal deformation”. *Advances in Space Research,* **46**(2), 236-249.
Nikaein, T., Iannini, L., Molijn, R. A., & Lopez-Dekker, P. (2021). “On the Value of Sentinel-1 InSAR Coherence Time-Series for Vegetation Classification”. *Remote Sensing,* **13**(16), 3300.
Ferretti, A., Prati, C., & Rocca, F. (1999). “Multibaseline InSAR DEM reconstruction: the wavelet approach”. *IEEE Transactions on Geoscience and Remote Sensing*, **37**(2), 705 - 715.
Bayer, B., Schmidt, D., & Simoni, A. (2017). “The Influence of External Digital Elevation Models on PS-InSAR and SBAS Results: Implications for the Analysis of Deformation Signals Caused by Slow Moving Landslides in the Northern Apennines (Italy)”. *IEEE Transactions on Geoscience and Remote Sensing*, **55**(5), 2618-2631.
Zhang, J., Gao, J., & Gao, F. (2024). “Time series land settlement monitoring and prediction based on SBAS-InSAR and GeoTemporal transformer model”. *Earth Science Informatics,* **17**, 5899-5911.
Zhang, L., Dai, K., Deng, J., Ge, D., Liang, R., Li, W., & Xu, Q. (2021). “Identifying Potential Landslides by Stacking-InSAR in Southwestern China and Its Performance Comparison with SBAS-InSAR”. *Remote Sensing,* **13**(18), 3662.
Aksoy, C. O. (2008). “Chemical injection application at tunnel service shaft to prevent ground settlement induced by groundwater drainage: A case study”. *International Journal of Rock Mechanics and Mining Sciences*, **45**(3), 376-383.
Zhang, L., Goh, A. T. C., Zhang, M., & Jin, D. (2017). “Intelligent Approach to Estimation of Tunnel-Induced Ground Settlement Using Wavelet Packet and Support Vector Machines”. *Journal of Computing in Civil Engineering*, **31**(2), 04016053.
Zhao, R., Li, Z.-W., Feng, G.-C., Wang, Q.-J., & Hu, J. (2016). “Monitoring surface deformation over permafrost with an improved SBAS-InSAR algorithm: With emphasis on climatic factors modeling”. *Remote Sensing of Environment,* **184**, 276-287.

Berardino, P., Fornaro, G., Lanari, R., & Sansosti, E. (2002). “A new algorithm for surface deformation monitoring based on small baseline differential SAR interferograms”. *IEEE Transactions on geoscience and remote sensing*, **40**(11), 2375-2383.
Du, Y., Yan, S., Yang, H., Jiang, J., & Zhao, F. (2021). “Investigation of deformation patterns by DS-InSAR in a coal resource-exhausted region with Spaceborne SAR imagery”. *Journal of Asian earth sciences: X*, **5**, 100049.
Tao, Q., Ding, L., Hu, L., Chen, Y., & Liu, T. (2020). “The performance of LS and SVD methods for SBAS InSAR deformation model solutions”. *International Journal of Remote Sensing*, **41**(22), 8547-8572.
Casu, F., Manzo, M., & Lanari, R. (2006). “A quantitative assessment of the SBAS algorithm performance for surface deformation retrieval from DInSAR data”. *Remote Sensing of Environment*, ***102*****(**3-4), 195-210.

RB, C. (1990). “STL: A seasonal-trend decomposition procedure based on loess”. *J Off Stat*, **6**, 3-73.

Araghi, A., Mousavi-Baygi, M., Adamowski, J., & Martinez, C. (2017). "Association between three prominent climatic teleconnections and precipitation in Iran using wavelet coherence". *International Journal of Climatology*, **37**(6), 2809-2830.

Komasi, M., Sharghi, S., & Safavi, H. R. (2018). "Wavelet and cuckoo search-support vector machine conjugation for drought forecasting using Standardized Precipitation Index (case study: Urmia Lake, Iran)". *Journal of Hydroinformatics*, **20**(4), 975-988.

Nazari-Sharabian, M., & Karakouzian, M. (2020). "Relationship between sunspot numbers and mean *annual precipitation: application of cross-wavelet transform—a case study". J,* **3**(*1), 7.*